

# Synthesis, structure and magnetism of the new $S = \frac{1}{2}$ kagome magnet $\text{NH}_4\text{Cu}_{2.5}\text{V}_2\text{O}_7(\text{OH})_2\cdot\text{H}_2\text{O}$

E Connolly<sup>1</sup>, P Reeves<sup>1,2</sup>, D Boldrin<sup>3</sup> and A S Wills<sup>1</sup>

<sup>1</sup> Department of Chemistry, University College London, 20 Gordon St, London WC1H 0AJ

<sup>2</sup> Present address: Department of Material Science and Metallurgy, University of Cambridge, 27 Charles Babbage Road, Cambridge CB3 0FS, UK

<sup>3</sup> Department of Physics, Imperial College, Prince Consort Road, London SW7 2BZ, UK

E-mail: a.s.wills@ucl.ac.uk

**Abstract.** The study of quantum spin-liquid states (QSL) with lattice dimension  $> 1$  has proven an enduring problem in solid state physics. Key candidate materials are the  $S = \frac{1}{2}$  kagome magnets due to their ability to host quantum fluctuations within the high degeneracy of their frustrated geometries. Studies of an increasing library of known  $S = \frac{1}{2}$  kagome magnetic materials has challenged our understanding of the possible QSL states, for example, the recent discovery of a chiral spin-liquid ground state in kapellasite showed that even magnets with ferromagnetic nearest-neighbour exchange are not necessarily trivial and that QSL states beyond the superposition of simple singlet are possible.

Here, we outline the synthesis, structure and preliminary magnetic characterisation of a candidate QSL material, the  $S = \frac{1}{2}$  kagome magnet  $\text{NH}_4\text{Cu}_{2.5}\text{V}_2\text{O}_7(\text{OH})_2\cdot\text{H}_2\text{O}$ . The crystal structure of  $\text{NH}_4\text{Cu}_{2.5}\text{V}_2\text{O}_7(\text{OH})_2\cdot\text{H}_2\text{O}$  has the 3-fold symmetry of a geometrically ‘perfect’ kagome lattice while the magnetism shows a competition between ferromagnetic and antiferromagnetic characters reminiscent of kapellasite.

Submitted to: *J. Phys.: Condens. Matter*

## 1. Introduction

The quest to discover what ground states occur when quantum fluctuations destabilize conventional magnetic order has become one of the backbones of modern condensed matter physics. Much of this work has focused on  $S = \frac{1}{2}$  kagome magnets, where the moment-bearing ions make up a 2-dimensional network of vertex-sharing triangles. Unlike the ground states of square and triangular  $S = \frac{1}{2}$  Heisenberg magnets, the  $S = \frac{1}{2}$  kagome Heisenberg antiferromagnet was shown theoretically not to order into a Néel state, even at  $T = 0$  K[1, 2, 3]. Research into these quantum frustrated magnets has largely followed the picture of the ground states being dynamic superposition states of degenerate local- or long-range entangled singlet pairs (Figure 1), quantum spin liquids

(QSLs). QSLs differ fundamentally from conventional magnetic order in that they do not break translational or rotational symmetry, but are instead defined by topological order parameters [4].

Recent experimental and theoretical investigations into  $S = \frac{1}{2}$  kagome magnets have revealed that new types of QSL states are able to form when nearest-neighbour ferromagnetic exchange is frustrated by antiferromagnetic further-neighbour interactions[5, 6], thereby expanding the field from one that was thought to be only relevant for nearest-neighbour antiferromagnets to those with competing signs of exchange. This work, focused on kapellasite ( $\alpha - \text{ZnCu}_3(\text{OH})_6\text{Cl}_2$ ) - which has a 12-sublattice chiral spin-liquid (cuboc2) ground state [5] - and its isostructural and isomagnetic analogue haydeeite ( $\alpha - \text{MgCu}_3(\text{OH})_6\text{Cl}_2$ ) helped formulate a new phase diagram for the QSL ground state involving a diagonal exchange integral. Changes in its value caused by differences in the bonding around their diamagnetic ions ( $\text{Mg}^{2+}$  and  $\text{Zn}^{2+}$ ), is able to drive the conventional ferromagnetic ordering seen in haydeeite into the 12-sublattice chiral spin-liquid (cuboc2) ground state[5, 6, 7, 8, 9].

At present, much of the research into experimental  $S = \frac{1}{2}$  kagome magnets is based on two main families of crystal structures: the atacamites (herbertsmithite  $\gamma - \text{ZnCu}_3(\text{OH})_6\text{Cl}_2$ , kapellasite  $\alpha - \text{ZnCu}_3(\text{OH})_6\text{Cl}_2$  and their isomagnetic relatives ‘Mg-herbertsmithite’  $\gamma - \text{MgCu}_3(\text{OH})_6\text{Cl}_2$ , and haydeeite  $\alpha - \text{MgCu}_3(\text{OH})_6\text{Cl}_2$ ) and the copper vanadates (volborthite  $\alpha - \text{Cu}_3\text{V}_2\text{O}_7(\text{OH}) \cdot 2\text{H}_2\text{O}$ , vesignieite  $\text{BaCu}_3\text{V}_2\text{O}_8(\text{OH})_2$  and ‘Sr-vesignieite’  $\text{SrCu}_3\text{V}_2\text{O}_8(\text{OH})_2$ ). The differences between these magnets has been revealing. The atacamites all have 3-fold symmetry, a quality that brings them close to the theoretical models. In the well studied herbertsmithite, the QSL state survives Dzyaloshinskii-Moriya (DM) anisotropy as the anisotropic exchange is largely axial and its strength is below a quantum critical point,  $D_z^C/J \simeq 0.1$ . In contrast, the DM component in vesignieite is dominated by the in-plane component,  $D_p$  [10, 11], despite  $D_z/J$  being similar to herbertsmithite, and this induces partial ferromagnetic order[11]. Even closely related materials can show wildly different behaviours, such as the QSL of dynamic singlets of herbertsmithite and of cuboc2 spin correlations in its polymorph kapellasite. At the root of this richness of properties are often subtleties in the crystal structure, such as variation in bond angles related to site disorder or differences in orbital ordering patterns and consequent superexchange pathways, as seen in volborthite[12], vesignieite[13, 14] and ‘Sr-vesignieite’[6].

Here, we present the synthesis, structure and preliminary magnetic measurements of a new  $S = \frac{1}{2}$  kagome material  $\text{NH}_4\text{Cu}_{2.5}\text{V}_2\text{O}_7(\text{OH})_2 \cdot \text{H}_2\text{O}$  based on the copper vanadates, and introduce its magnetic properties.

## 2. Synthesis

Syntheses using a scaled down version (to 30 % of the literature quantities) of that previously given in a paper by Palacio[15] at  $T = 170^\circ\text{C}$ , produced a product contaminated by an amorphous impurity phase and crystalline  $\text{NH}_4\text{VO}_3$ . The latter

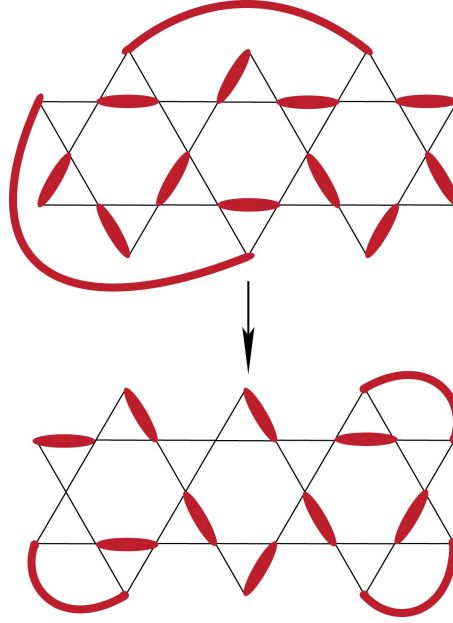
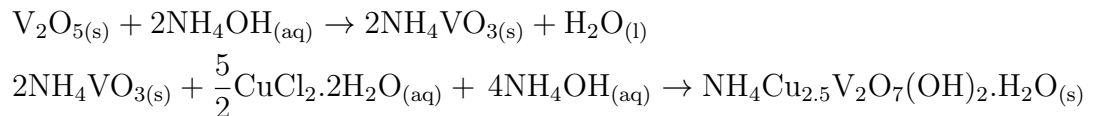


**Figure 1.** Schematic of a kagome structure hosting a QSL state. The short and long range entangled spins are highlighted in red. The entangled singlet states are in a disordered arrangement over the kagome lattice. The degeneracy of the ground state allows for zero-point energy fluctuations to other disordered arrangements.

could be identified by a peak in the diffraction data at  $2\theta = 24^\circ$  that is also visible in [15].

Further studies showed that the impurities form at  $T \leq 80^\circ\text{C}$  and  $T \geq 130^\circ\text{C}$ . A phase pure sample was obtained as follows:  $\text{NH}_4\text{OH}$  (0.62 ml, 32 % wt, Sigma-Aldrich) was diluted with distilled water (3.88 ml). To this solution,  $\text{V}_2\text{O}_5$  (166 mg, 99.6 %, Aldrich) was added and the suspension was stirred for 1 hour, whereupon it turned yellow. Finally,  $\text{CuCl}_2 \cdot 2\text{H}_2\text{O}$  (311 mg, 99.8 %, Aldrich) dissolved in distilled water (3.0 ml), was added to the yellow suspension. This was then stirred for 1 hour to homogenize, producing a turquoise gel. The gel was loaded into a Pyrex pressure tube (15 ml, Ace Glass Inc.) and then suspended in a silicon oil bath at  $115^\circ\text{C}$  for 24 hours. The product was washed 3 times in water *via* centrifugation ( $4.5 \times 10^3$  rpm, 2 mins) and dried at  $60^\circ\text{C}$  for 5 hours. A yellow powder of  $\text{NH}_4\text{Cu}_{2.5}\text{V}_2\text{O}_7(\text{OH})_2 \cdot \text{H}_2\text{O}$  was produced in a yield of  $\sim 44\%$ .

The ratios of the final reagent used are 1  $\text{V}_2\text{O}_5$  : 2  $\text{CuCl}_2 \cdot 2\text{H}_2\text{O}$  : 6  $\text{NH}_4\text{OH}$  : 422  $\text{H}_2\text{O}$ . Powder XRD indicated that the product of the first reaction is  $\text{NH}_4\text{VO}_3$ . The pH of the second reaction was 9.6 before and after the synthesis. We propose the following reaction mechanism for the formation of  $\text{NH}_4\text{Cu}_{2.5}\text{V}_2\text{O}_7(\text{OH})_2 \cdot \text{H}_2\text{O}$ :



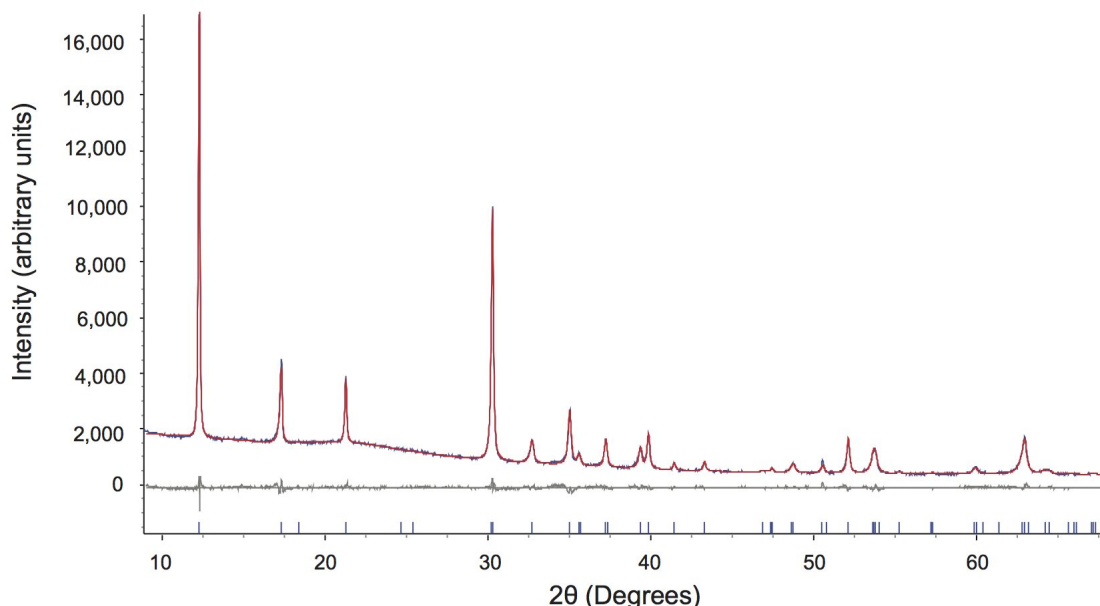
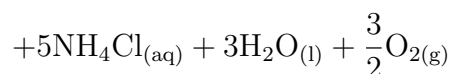


**Figure 2.** Rietveld refinement of XRD data measured on a powdered sample of  $\text{NH}_4\text{Cu}_{2.5}\text{V}_2\text{O}_7(\text{OH})_2 \cdot \text{H}_2\text{O}$  at a wavelength of  $\lambda = 1.5406 \text{ \AA}$ . The red, blue and grey lines, and blue markers represent the fit, data, difference plot and reflection positions, respectively. The final goodness-of-fit parameter was  $\chi^2 = 2.35$  with 56 variables.



The hypothesized reaction scheme has a calculated reagent ratio for 1 M of  $\text{NH}_4\text{Cu}_{2.5}\text{V}_2\text{O}_7(\text{OH})_2 \cdot \text{H}_2\text{O}$  of 1  $\text{V}_2\text{O}_5$  : 2.5  $\text{CuCl}_2 \cdot 2\text{H}_2\text{O}$  : 6  $\text{NH}_4\text{OH}$ , indicating that our synthetic conditions correspond to a slight deficit of  $\text{CuCl}_2 \cdot 2\text{H}_2\text{O}$ . The outlined synthetic procedure can be used to understand how variation to concentrations or reagent types will effect the product.

### 3. Crystal structure determination

The powder XRD data was recorded on a STOE Stadi-P diffractometer using  $\text{Cu-K}\alpha_1$  radiation ( $\lambda = 1.5406 \text{ \AA}$ ) with a rotating capillary sample holder. As no crystal structure is known for  $\text{NH}_4\text{Cu}_{2.5}\text{V}_2\text{O}_7(\text{OH})_2 \cdot \text{H}_2\text{O}$ , the starting lattice parameters, space group and atomic positions for the crystal structure model were based on the engelhauptite ( $\text{KCu}_3\text{V}_2\text{O}_7(\text{OH})_2\text{Cl}$ ) structure in the  $P6_3/mmc$  space group[16]. The Rietveld refinement was carried out using the TOPAS software package[17]. The data, final calculated and difference plots are shown in Figure 2. The crystal structure data obtained from the refinement is displayed in Table 1; details of the data collection procedure and refinement are given in the supplementary information. All crystal structure figures were produced using VESTA [18].

Atom	Wyckoff site	$x$	$y$	$z$	$B_{\text{iso}} (\text{\AA}^2)$	Occ.
Cu	$6g$	$\frac{1}{2}$	$\frac{1}{2}$	0	4.1(11)	0.7294(68)
V	$4e$	0	0	0.37355(19)	2.5(11)	1
O(1)	$12k$	0.15623(87)	0.3125(17)	0.59043(31)	3.4(11)	1
O(2)	$2b$	0	0	$\frac{1}{4}$	5.0(11)	1
O(H)	$4f$	$\frac{1}{3}$	$\frac{2}{3}$	0.06520(61)	2.1(10)	1
O(w)	$6h$	0.74537	0.3707(98)	$\frac{3}{4}$	5.8(75)	0.242(25)
N	$4f$	$\frac{1}{3}$	$\frac{2}{3}$	0.2551(19)	2.1(20)	0.417(21)
H(1)	$4f$	$\frac{1}{3}$	$\frac{2}{3}$	0.61500	5.7 [19]	1
H(2)	$24l$	0.64126	0.44028	0.76082	5.7 [19]	$= \frac{O_{w_{\text{occ}}}}{2}$
H(3)	$12k$	0.18614	0.59307	0.74228	5.7 [19]	$= N_{\text{occ}}$
H(4)	$4f$	$\frac{1}{3}$	$\frac{2}{3}$	0.81662	5.7 [19]	$= \frac{N_{\text{occ}}}{2}$

Table 1: The crystal structure data for  $\text{NH}_4\text{Cu}_{2.5}\text{V}_2\text{O}_7(\text{OH})_2 \cdot \text{H}_2\text{O}$  displaying the atom, Wyckoff site, atomic coordinates, thermal parameter and occupancies.

### 3.1. Structural characterization

$\text{NH}_4^+$  and  $\text{H}_2\text{O}$  were assigned respectively to the framework cavities occupied by  $\text{K}^+$  and  $\text{Cl}^-$  in the similarly structured engelhauptite [16]. Structural refinements indicated that these sites feature significant disorder which was modeled by lowering the symmetry of the N site from  $2d$  to  $4f$  and the O(w) site from  $2c$  to  $6h$ . To help reveal how hydrogen bonding could stabilise the positions of these species, rigid bodies were defined with the bond lengths and angles set as the following for  $\text{NH}_4^+$ :  $\text{N-H}(3,4) = 0.974 \text{ \AA}$ ,  $\angle \text{H}(3,4)\text{-N-H}(3,4) = 109.5^\circ$  [20], and for  $\text{H}_2\text{O}$  and the  $\text{OH}^-$  group:  $\text{O(w)-H}(2) = 1.019 \text{ \AA}$ ,  $\text{O(H)-H}(1) = 1.008 \text{ \AA}$  and  $\angle \text{H}(3)\text{-O(w)-H}(3) = 109.5^\circ$  [19]

During the refinement, the site occupancy of the divanadate and hydroxide groups were fixed to be unity while the occupancies of the  $\text{Cu}^{2+}$ ,  $\text{NH}_4^+$  and  $\text{H}_2\text{O}$  groups were freely refined. The refined structural formula is  $(\text{NH}_4)_{0.834}\text{Cu}_{2.188}\text{V}_2\text{O}_7(\text{OH})_2 \cdot 0.726(\text{H}_2\text{O})$ , indicating that some loss of  $\text{Cu}^{2+}$  occurs that is presumed to be charge compensated by protonation of the water molecules to form hydronium ions. (The latter cannot be distinguished from these data.)

### 3.2. Structural analysis

Selected bond distances and angles which are pertinent to the description and discussion of the structure of  $\text{NH}_4\text{Cu}_{2.5}\text{V}_2\text{O}_7(\text{OH})_2 \cdot \text{H}_2\text{O}$  are displayed in Table 2 and the refined structure viewed along the  $a$ - and  $c$ - axes is displayed in Fig 3. The magnetic moments reside on brucite-type Cu-octahedra sheets that are separated by pyrovanadate pillars and interstitial pores, the latter contain  $\text{NH}_4^+$  and  $\text{H}_2\text{O}$ . The interlayer Cu-Cu separation of  $7.22 \text{ \AA}$  is very similar to that of volborthite [19] ( $7.21 \text{ \AA}$ ) suggesting that the superexchange between layers will be very weak and the magnetic Hamiltonian will

Interatomic distances (Å)		Angles (°)	
Cu-O(H)	1.9373(44)	Cu-O(H)-Cu	99.54(29)
Cu-O(1)	2.1881(43)	Cu-O(1)-Cu	85.05(21)
		O(1)-Cu-O(1)	91.63(38)
		O(H)-Cu-O(1)	92.48(20)
V-O(2)	1.7867(25)	V-O(2)-V	180.00
V-O(1)	1.6881(78)	O(2)-V-O(1)	108.19(19)
		O(1)-V-O(1)	110.72(17)
N-H(4)···O(1)	2.182(73)		
N-H(3)···O(w)	2.060(69)		
O(H)-H(1)···O(w)	1.749(21)		

Table 2: Selected bond distances and angles from the structure of  $\text{NH}_4\text{Cu}_{2.5}\text{V}_2\text{O}_7(\text{OH})_2\cdot\text{H}_2\text{O}$

be highly 2-dimensional. The stacking of the kagome layers differs for the 2 materials - in volborthite they are in phase while those of  $\text{NH}_4\text{Cu}_{2.5}\text{V}_2\text{O}_7(\text{OH})_2\cdot\text{H}_2\text{O}$  are staggered.

The  $\text{Cu}^{2+}$  ions lie on a  $2/m$  point symmetry site to form an isotropic kagome lattice, made up of identical equilateral triangular units ( $\text{Cu-Cu}=2.958$  Å). The isotropic kagome lattice has a ground state Hamiltonian with few exchange terms which better simulates the simple model of theory.

The Cu on the  $6g$  site was freely refined to an occupancy of  $\sim 73\%$ , a notable deviation from the idealised level that would reduce the number of resonant states available to a QSL state[21]. Despite this, the occupancy is still higher than the bond percolation threshold for a kagome ( $p_c^{\text{bond}}=52\%$ ) [22]. Further, this situation does not necessarily exclude the possibility of a QSL state as further neighbour entanglement may still cause sufficient degeneracies to allow one to occur. We note that similar levels of site disorder are seen in some kapellasite samples where they do not to destroy its QSL ground state [5].

The Cu-Cu nearest-neighbour superexchange interactions in  $\text{NH}_4\text{Cu}_{2.5}\text{V}_2\text{O}_7(\text{OH})_2\cdot\text{H}_2\text{O}$  are mediated by a O(H) group which sits on a 3-fold axis with a mirror plane, and O(1) which also lies on a mirror plane. The bridging angles of  $\angle \text{Cu-O(H)-Cu} = 99.54(29)^\circ$  and  $\angle \text{Cu-O(1)-Cu} = 85.05(21)^\circ$  are expected to mediate antiferromagnetic and ferromagnetic exchange, respectively, based on the Goodenough-Kanamori-Anderson rules [23, 24]. Weak exchange interactions can be expected through both of these pathways as they are close to the cross-over angle at  $90^\circ$  that is a minimum in both ferromagnetic and antiferromagnetic exchange. Such a situation increases the importance of other low-energy exchange terms to the magnetic ground state, illustrated by Dzyaloshinskii-Moriya exchange's role in forming vesignieite's unique frozen and dynamic spin ground state [11]. The Cu-O bond distances in  $\text{NH}_4\text{Cu}_{2.5}\text{V}_2\text{O}_7(\text{OH})_2\cdot\text{H}_2\text{O}$  and the angles involved in superexchange across the kagome lattice are strikingly similar to those of vesignieite, Table 3. As both materials are then expected to display similar magnetic properties, the Dzyaloshinskii-Moriya exchange is also likely to be important here.

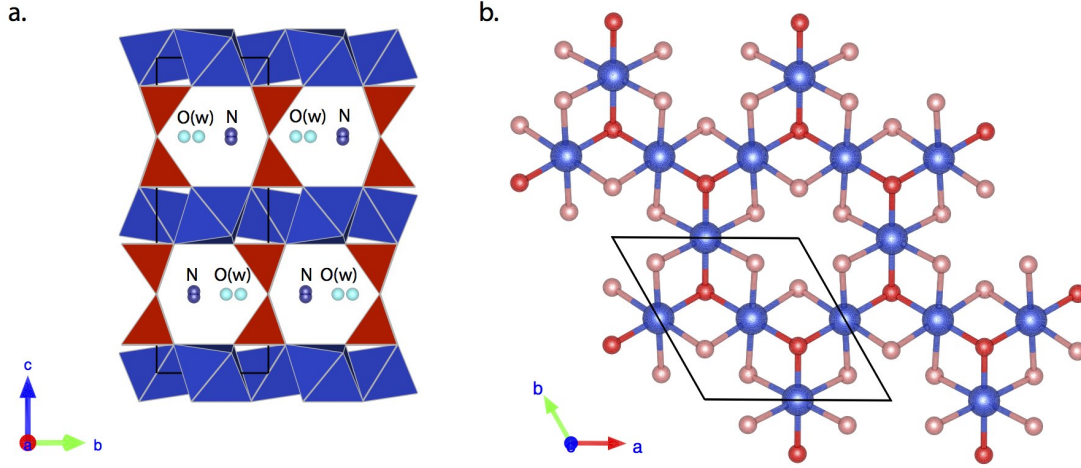


**Figure 3.** **a.** The structure of  $\text{NH}_4\text{Cu}_{2.5}\text{V}_2\text{O}_7(\text{OH})_2 \cdot \text{H}_2\text{O}$  observed down the  $a$ -axis. The Cu-octahedra sheets and bivanadate layers are illustrated in blue and red, respectively. The oxygen of the  $\text{H}_2\text{O}$  and the nitrogen of the  $\text{NH}_4^+$  are shown in the interstitial sites. **b.** The kagome plane viewed down the  $c$ -axis. The  $\text{Cu}^{2+}$  ions (black) sit on a  $6g$  site of the  $P6_3/mmc$  space group which has 3-fold rotational symmetry and so the  $\text{Cu}^{2+}$  ions form a ‘perfect’ kagome. The  $\text{Cu}^{2+}$  ions ferromagnetic and antiferromagnetic superexchange pathways *via* the O(2) (red) and O(H) (pink) species, respectively, are shown.

	$\text{NH}_4\text{Cu}_{2.5}\text{V}_2\text{O}_7(\text{OH})_2 \cdot \text{H}_2\text{O}$ $P6_3/mmc$	$\text{BaCu}_3\text{V}_2\text{O}_8(\text{OH})_2$ $C2/m$	$\text{BaCu}_3\text{V}_2\text{O}_8(\text{OH})_2$ $P3_121$
Cu–O(H)	1.93691(63) Å	1.913(2) Å	1.91051(74)
Cu–O	2.18777(84) Å	2.183(2) Å	2.07250(28) / 2.14803(75)
$\angle$ Cu–O(H)–Cu	99.54(29) °	101.7(4) °	103.15(66)
$\angle$ Cu–O–Cu	85.05(21) °	85.6(9) °	92.94(34) / 83.47(54)

Table 3: Cu–O bond distances and angles for  $\text{NH}_4\text{Cu}_{2.5}\text{V}_2\text{O}_7(\text{OH})_2 \cdot \text{H}_2\text{O}$  and two structures of vesignieite which mediate superexchange are listed for comparison: the crystal structure of vesignieite is disputed so comparisons were drawn with both the monoclinic  $C2/m$  [25] and trigonal  $P3_121$  [26] structures; equivalent bond distances and bond angles from each structure have been compared. Some oxygens in the  $P3_121$  structure exhibit disorder over multiple sites; two values have been stated for bond lengths and angles formed with these oxygens.

An important structural feature that is seen in several of the Cu-vanadate kagome magnets [27, 28, 29] is an unusual axial compression [2+4] Jahn-Teller distortion[29], formed of 2 short axial bonds and 4 longer equatorial bonds: Cu–O(H)=1.9373(44) Å and Cu–O(1)= 2.1881(43) Å, respectively. At first sight, this configuration could taken to indicate localisation of the unpaired electron in the  $d_{x^2-y^2}$  orbital of  $\text{Cu}^{2+}$ , but it has been argued that this type of distortion in powder diffraction is

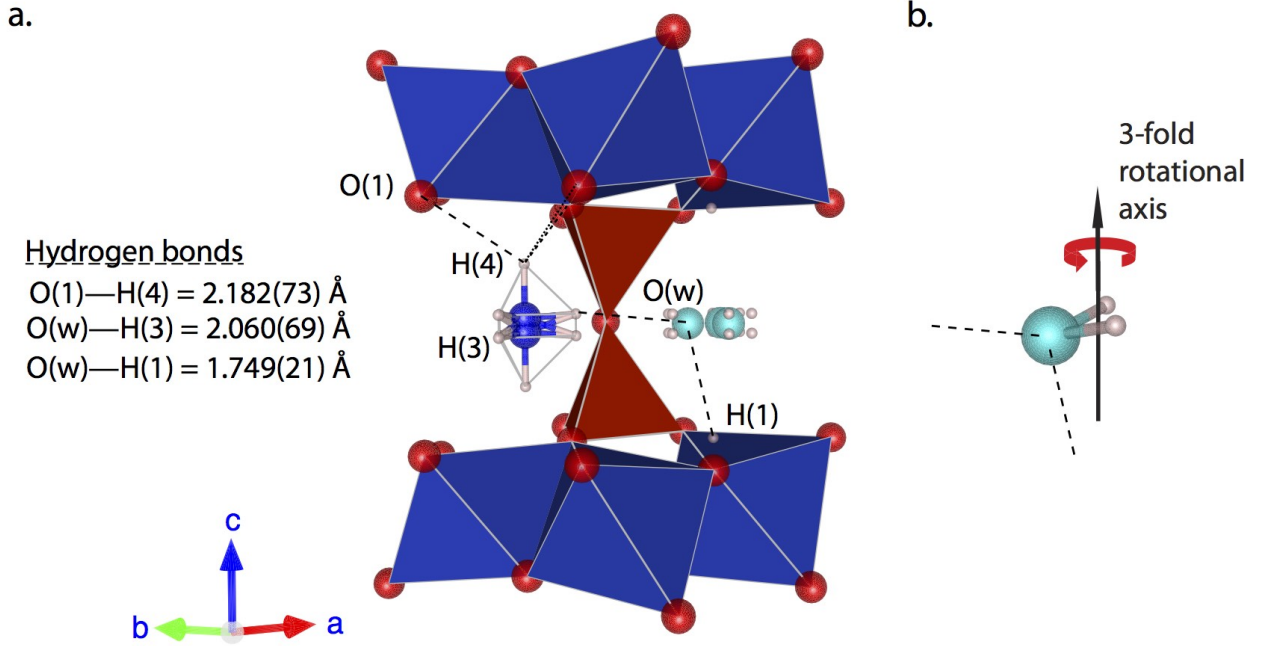


**Figure 4.** **a** The interstitial  $\text{NH}_4^+$  and  $\text{H}_2\text{O}$  molecules are displayed sitting on the disordered sites between the Cu-octahedra sheets that make up the kagome layers.  $\text{NH}_4^+$  has two equivalent energy orientations that are mirror images in the  $ab$ -plane. N-H(4) lies along the  $c$ -axis and forms three equivalent hydrogen bonds with O(1). The N-H(3) bonds lie on the planes of the 3-fold axis and H(3) forms a hydrogen bond with O(w); O(w) lies off the 3-fold axis and also hydrogen bonds to H(1). **b** A single  $\text{H}_2\text{O}$  rigid body is displayed with the hydrogens canted out of the  $ab$ -plane as observed in volborthite [12]: the lone pairs of O(w) are now pointing at H(1) for hydrogen bonding.

commonly an artifact of averaging when the half-occupied  $d_{z^2}$  orbital fluctuates between two degenerate orientations[30]. We therefore conclude that the Jahn-Teller effect of the  $\text{Cu}^{2+}$  ions in  $\text{NH}_4\text{Cu}_{2.5}\text{V}_2\text{O}_7(\text{OH})_2 \cdot \text{H}_2\text{O}$  is dynamic at room temperature and that the  $\text{Cu}^{2+}$  orbitals fluctuate.

Our refinements also show that the  $\text{NH}_4^+$  unit is displaced from the high symmetry  $2d$  site along the  $c$ -axis; this displacement is likely stabilized by the formation of 3 equivalent N-H(4)···O(1) = 2.182 Å hydrogen bonds and a linear N-H(3)···O(w) = 2.060 Å (Figure 4). In turn, displacement of the  $\text{H}_2\text{O}$  from the  $2c$  site is such that the hydrogens point below the  $ab$ -plane of the O(w) site, as is also observed in volborthite [12], which would allow the lone pair orbitals of O(w) to point towards H(1), forming O(H)-H(1)···O(w) = 1.987 Å. The orientations of these extra-framework molecules could be confirmed through neutron diffraction on a deuterated sample.

#### 4. Magnetic characterisation

Zero-field cooled magnetisation data were collected from  $\text{NH}_4\text{Cu}_{2.5}\text{V}_2\text{O}_7(\text{OH})_2 \cdot \text{H}_2\text{O}$  (65.3 mg) using the vibrating sample magnetometer of a Quantum Design PPMS-



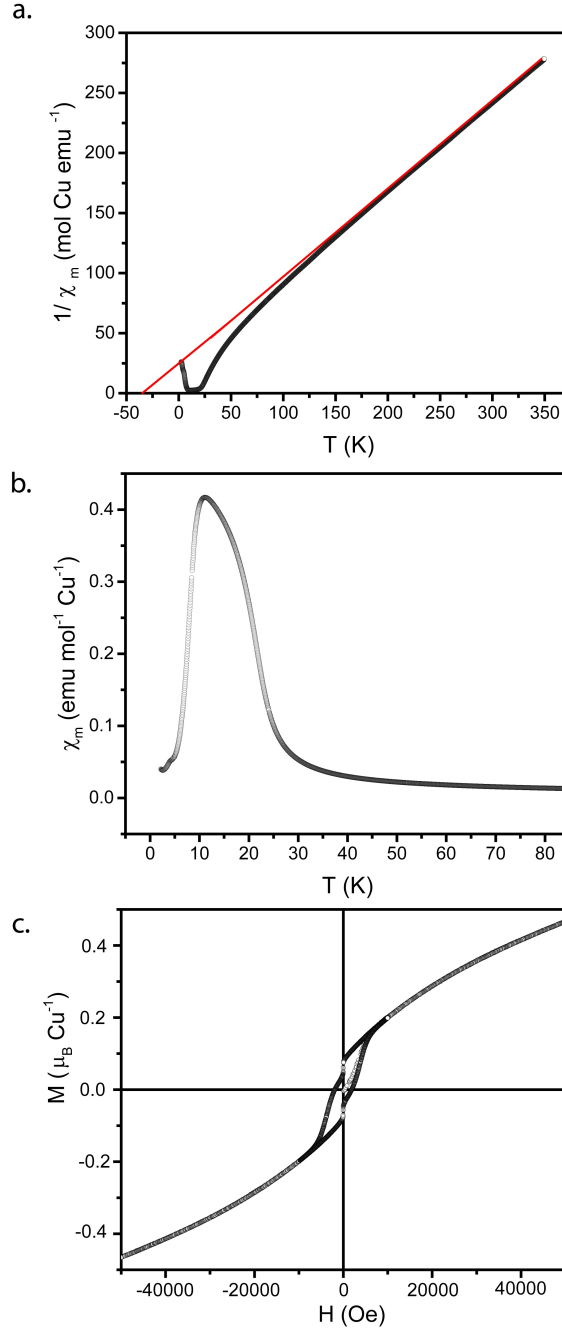


**Figure 5.** All magnetization data was collected on a zero-field cooled sample of  $\text{NH}_4\text{Cu}_{2.5}\text{V}_2\text{O}_7(\text{OH})_2 \cdot \text{H}_2\text{O}$ . **a.** The  $\chi_m^{-1}$  vs  $T$  plot shows a deviation from the linear Curie-Weiss law at  $T \leq 170$  K due to a build up of local spin correlations. Extrapolation from the linear slope yields a Weiss temperature of  $\theta_W \simeq -30$  K indicating antiferromagnetic exchange, the absence of an antiferromagnetic transition at  $T = 30$  K indicates a frustration of magnetic ordering characteristic of quantum kagome magnets. **b.** A plot of  $\chi_m$  vs  $T$  shows a ferromagnetic transition at  $T_C \sim 17$  K. **c.**  $M$  vs.  $H$  at 2 K hysteresis loop with steps, confirming ferromagnetic ordering and indicating a build up of magnetic domains.

9T in a field of 1000 Oe and with heating rate of 2 K/min. Inspection of  $\chi$  vs.  $T$  indicates that there is a ferromagnetic-like transition at  $T_C \sim 17$  K that leads to a broad maximum, while the temperature-dependence of the inverse susceptibility shows a linear Curie-Weiss regime over the range  $170 \leq T \leq 400$  K from which a Weiss temperature of  $\theta_W \simeq -30$  K can be extrapolated. The deviation from linear behaviour on cooling below 170 K indicates that while spin correlations are building up, ordering is suppressed to a temperature below  $T = |\theta_W|$ : a well known characteristic of  $S = \frac{1}{2}$  frustrated magnets[31, 7, 9]. The juxtaposition of a ferromagnetic-like transition and a negative Weiss temperature indicates there is a competition within the magnetism of  $\text{NH}_4\text{Cu}_{2.5}\text{V}_2\text{O}_7(\text{OH})_2 \cdot \text{H}_2\text{O}$ . The dominant character of the mean field appears to be antiferromagnetic and the transition only occurs when a ferromagnetic energy scale becomes relevant. The room temperature value of the effective moment,  $\mu_{\text{eff}} = 2.06 \mu_B$ , is higher than the spin-only value of  $\mu_{\text{eff}} = 1.73 \mu_B$  indicating that the Landé g-factor for  $\text{Cu}^{2+}$  exceeds 2 and that there is an orbital contribution to the magnetism[10].

Hysteresis in the magnetic field-dependence of the magnetisation data at 2 K shown in Figure 5c confirms a coherent ferromagnetic component in the low temperature state and an unsaturated paramagnetic signal up to 5 T. The coexistence of ferromagnetic and paramagnetic signals has been observed for some other  $S = \frac{1}{2}$  kagome magnets, namely vesignieite, haydeeite, and ‘Mg-herbertsmithite’ [32, 9, 33]. The contribution of the ferromagnetic and paramagnetic signals to the hysteresis were previously isolated for haydeeite using a paramagnetic Brillouin function with a constant term that accounts for the ferromagnetic response [26]. In order to extract the ferromagnetic contribution and obtain a value of the spontaneous magnetisation independent of a paramagnetic signal the following equation was used to fit the hysteresis data for  $\text{NH}_4\text{Cu}_{2.5}\text{V}_2\text{O}_7(\text{OH})_2 \cdot \text{H}_2\text{O}$ :

$$M(H)/M_{\text{sat}} = (1 - f)B_{\text{J,PM}}(H) + f \quad (1)$$

where  $M_{\text{sat}}$  is the saturated magnetisation,  $f$  is the ferromagnetic response constant and  $B_{\text{J,PM}}$  is the paramagnetic Brillouin function per molecule,

$$B_{\text{J,PM}}(H) = \tanh(g\mu_B JH/k_B T) \quad (2)$$

Taking  $\text{Cu}^{2+}$  to be spin only,  $J = S = \frac{1}{2}$ ,  $g$  and  $f$  were refined to fit the high-field curve and yielded values of  $g = 2.36$  and  $f = 0.41$ . This latter value indicates that  $\sim 41\%$  of spins are frozen. A plot of the extracted ferromagnetic contribution to the hysteresis is shown in Figure 6a, and steps in the hysteresis are clearly illustrated in Figure 6b. Magnification of one step, shown in figure 6c, illustrates the sensitivity of the measured moment to small changes of field over the range  $-50 \text{ Oe} \lesssim H \lesssim 50 \text{ Oe}$ . This behaviour makes it difficult to determine the spontaneous moment as zero field coincides with the approximate center of the step, but an upper limit of  $\leq 0.075 \mu_B \text{ Cu}^{-1}$  is estimated. The steps in the hysteresis are unusual and are not observed for any other  $S = \frac{1}{2}$  kagome

magnets, indicating that the magnetic ground state is indeed exotic and warrants further investigation.

As discussed in section 3.2,  $\text{NH}_4\text{Cu}_{2.5}\text{V}_2\text{O}_7(\text{OH})_2 \cdot \text{H}_2\text{O}$  and vesignieite have very similar superexchange pathways and are expected to display similar magnetic properties. Indeed, both feature antiferromagnetic Weiss temperatures, of  $\theta_W \simeq -85(5)$  K and  $\theta_W \simeq -30$  K [14], respectively, and have magnetic transitions involving a ferromagnetic component [32] to a state with a similar proportion of frozen spins at  $T \leq 2$  K [14].  $\text{V}^{51}$  NMR and  $\mu\text{SR}$  studies of vesignieite have indicated that the spin ordering of only partial ( $\sim 40\%$ ) below  $T_N = 9$  K and that a dynamic component remains down to 1 K [14, 34]. ESR analysis of vesignieite revealed that the ordered spin structure was induced by an in-plane Dyaloshinsky-Moriya and is canted out of the kagome plane [11].

A clear difference between the materials is the observed step structure in the hysteresis of  $\text{NH}_4\text{Cu}_{2.5}\text{V}_2\text{O}_7(\text{OH})_2 \cdot \text{H}_2\text{O}$ . This may be characteristic of a spin reorientation transition, of the type seen in the metallic kagome ferromagnetic  $\text{Fe}_3\text{Sn}_2$  [35], though here it is unclear whether it would be continuous or involve a 1<sup>st</sup> order transition and changes in domain occupation.

## 5. Conclusion

A hydrothermal synthesis and reaction mechanism for the production of pure crystalline samples of the new kagome magnet  $\text{NH}_4\text{Cu}_{2.5}\text{V}_2\text{O}_7(\text{OH})_2 \cdot \text{H}_2\text{O}$  has been outlined. Its crystal structure consists of ‘perfect’  $\text{Cu}^{2+}$  kagome-planes that are separated by  $\text{V}_2\text{O}_7^{4-}$  pyrochlore pillars, with ammonium and water groups residing in the interstitial sites; the orientation of the interstitial molecule has been speculated upon.

Preliminary magnetization measurements indicate a suppression of magnetic ordering and superparamagnetic correlations that are characteristic of  $S = \frac{1}{2}$  kagome antiferromagnets, and a ferromagnetic transition at  $T_C \simeq 17$  K. Remarkably, steps are seen in the hysteresis data at low field which indicate that the ground state has a unusual and marked sensitivity to an applied magnetic field.

Structural and magnetic similarities between  $\text{NH}_4\text{Cu}_{2.5}\text{V}_2\text{O}_7(\text{OH})_2 \cdot \text{H}_2\text{O}$  and vesignieite suggest that an in-plane component to the Dyaloshinsky-Moriya exchange plays an important role in spin-ordering. We speculate that this may also involve an orbital freezing transition of the spin-bearing  $\text{Cu}^{2+}$  ion. Further studies by  $\mu\text{SR}$  and inelastic neutron scattering studies would help determine the ground state of this unusual kagome magnet and its location in the phase diagram of possible QSLs.

## 6. Acknowledgments

We would like to thank Jeremy Cockcroft for informative discussions, Martin Vickers for experimental assistance, and UCL for the provision of the studentship.

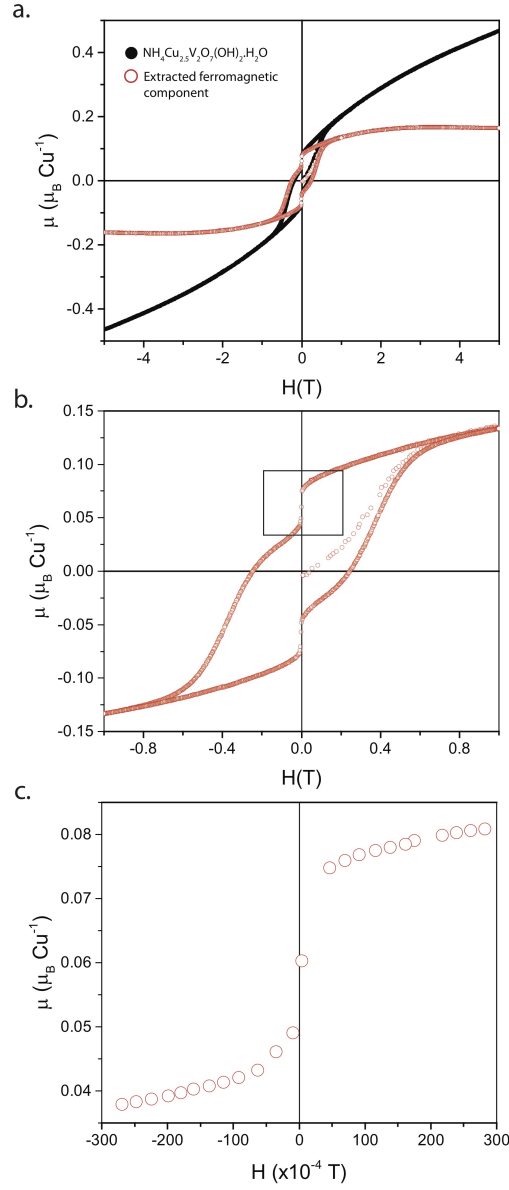


**Figure 6.** **a** The extracted ferromagnetic contribution (red circles) to the hysteresis is shown along with the  $M$  vs  $H$  data taken at 2 K (black circles) **b** The ferromagnetic hysteresis loop shows a step near zero-field. **c** A close up of region of the step shows it to occur between  $-50 \text{ Oe} \lesssim H \lesssim 50 \text{ Oe}$ .

## 7. References

- [1] Rokhsar D S and Kivelson S A 1988 *Phys. Rev. Lett.* **61** 2376–2379
- [2] Sachdev S 1992 *Phys. Rev. B* **45** 12377
- [3] Lecheminant P, Bernu B, Lhuillier C, Pierre L and Sindzingre P 1997 *Phys. Rev. B* **56** 2521
- [4] Balents L 2010 *Nature* **464** 199
- [5] Fåk B, Kermarrec E, Messio L, Bernu B, Lhuillier C, Bert F, Mendels P, Koteswararao B, Bouquet F, Ollivier J, Hillier A D, Amato A, Colman R H and Wills A S 2012 *Phys. Rev. Lett.* **109** 037208
- [6] Boldrin D, Fak B, Enderle M, Bieri S, Ollivier J, Rols S, Manuel P and Wills A S 2015 *Phys. Rev. B* **92**
- [7] Colman R H, Ritter C and Wills A S 2008 *Chem. Mat.* **20** 2005
- [8] Janson O, Richter J and Rosner H 2008 *Phys. Rev. Lett.* **101** 106403
- [9] Colman R, Sinclair A and Wills A S 2010 *Chem. Mat.* **22** 5774
- [10] Zorko A, Nellutla S, van Tol J, Brunel L C, Bert F, Duc F, Trombe J C, de Vries M A, Harrison A and Mendels P 2008 *Phys. Rev. Lett.* **101** 026405
- [11] Zorko A, Bert F, Ozarowski A, van Tol J, Boldrin D, Wills A S and Mendels P 2013 *Phys. Rev. B* **88** 144419
- [12] Hiroi Z, Hanawa M, Kobayashi N, Nohara M, Takagi H, Kato Y and Takigawa M 2001 *J. Phys. Soc. Jpn.* **70** 3377
- [13] Okamoto Y, Yoshida H and Hiroi Z 2009 *J. Phys. Soc. Jap.* **78** 3
- [14] Colman R H, Bert F, Boldrin D, Hillier A D, Manuel P, Mendels P and Wills A S 2011 *Phys. Rev. B* **83** 180416 ISSN 1098-0121
- [15] Palacio L A, Silva E R, Catalão R, Silva J M, Hoyos D A, Ribeiro F R and Ribeiro M F 2008 *J. Haz. Mat.* **153** 628
- [16] Pekov I V, Siidra O I, Chukanov N V, Yapaskurt V O, Britvin S N, Krivovichev S V, Schüller W and Ternes B 2015 *Min. Petro.* **3**
- [17] Bruker AXS 2008 Topas v4: General profile and structure analysis software for powder diffraction data
- [18] Momma K and Izumi F 2011 Vesta 3 for three-dimensional visualization of crystal, volumetric and morphology data
- [19] Lafontaine M A, Le Bail A and Ferey G 1990 *J. Sol. St. Chem.* **85** 220
- [20] Hawthorne F C 1977 *J. Sol. St. Chem.* **170** 157–170
- [21] Lacroix C, Mendels P and Mila F (eds) 2011 *Introduction to Frustrated Magnetism* (New York, USA: Springer)
- [22] Feng X, Deng Y and Blöte H W J 2008 *Phys. Rev. E* **78** 1–6
- [23] Goodenough J B 1955 *Phys. Rev.* **100** 564.
- [24] Kanamori J 1959 *J. Phys. Chem. Sol.* **10** 87
- [25] Zhesheng M 1991 *Acta Geo. Sin.* **4** 2
- [26] Boldrin D 2015 *Synthesis and Study of Quantum Kagome Magnets* Ph.D Thesis UCL
- [27] Yoshida H, Yamaura J I, Isobe M, Okamoto Y, Nilsen G J and Hiroi Z 2012 *Nat. Commun.* **3** 860
- [28] Okamoto Y, Yoshida H and Hiroi Z 2009 *J. Phys. Soc. Jap.* **78** 033701
- [29] Boldrin D and Wills A S 2015 *J. Mater. Chem. C* **3** 4308
- [30] Burns P and Hawthorne F 1996 *Can. Mineral.* **34** 1089
- [31] Hiroi Z, Yoshida H, Okamoto Y and Takigawa M 2009 *J. Phys. Conf. Ser.* **145** 012002
- [32] Yoshida H, Michiue Y, Takayama-Muromachi E and Isobe M 2012 *J. Mat. Chem.* **22** 18793
- [33] Colman R H, Sinclair A and Wills A S 2011 *Chem. Mat.* **23** 1811–1817
- [34] Quilliam J A, Bert F, Colman R H, Boldrin D, Wills A S and Mendels P 2011 *Phys. Rev. B* **84** 180401
- [35] Fenner L A, Dee A A and Wills A S 2009 *J Phys. Condens. Matter* **21** 452202
- [36] Stephens P W 1999 *J. App. Crys.* **32** 281
- [37] Roe R J and Krigbaum W R 1964 *J. Chem. Phys.* **40** 2608

*Synthesis, structure and magnetism of the new  $S = \frac{1}{2}$  kagome magnet  $NH_4Cu_{2.5}V_2O_7(OH)_2 \cdot H_2O$* 14

[38] Young R A 2001 *The Rietveld Method* (New York, USA: Oxford University Press)

## Appendix A. Supplementary information

Crystallographic data	
Chemical formula	$\text{NH}_4\text{Cu}_{2.5}\text{V}_2\text{O}_7(\text{OH})_2 \cdot \text{H}_2\text{O}$
Crystal system	Hexagonal
Space group	$P6_3/mmc$ (194)
$a$ (Å)	5.9159(2)
$c$ (Å)	14.4430(6)
Volume (Å <sup>3</sup> )	437.76(2)
Formula units ( $Z$ )	2
Data collection	
Radiation, $\lambda$ (Å)	CuK $\alpha$ 1, 1.54
$2\theta$ -step size increments (°)	0.05
$2\theta$ range (°)	9 - 70
Geometry	Debye-Scherrer geometry
Temperature (K)	293
Zero error (°)	0.04809(5)
$\mu\text{R}$	1.6(4)
Number of observed reflections	53
Refinement	
Instrumental, unit cell and profile parameters	36
Peak area parameters	20
Profile function	Stephens' anisotropic broadening [36] Spherical harmonics [37]
$R_{\text{exp}}$ [38]	1.43
$R_{\text{wp}}$ [38]	3.34
$\chi^2$ [38]	2.35

Table A1: Details of the data collection procedure and Rietveld refinement of  $\text{NH}_4\text{Cu}_{2.5}\text{V}_2\text{O}_7(\text{OH})_2 \cdot \text{H}_2\text{O}$  are displayed along with crystallographic data